








RESEARCH ARTICLE | NOVEMBER 17 2023

Numerical investigation of oblique detonation waves on a truncated cone in hydrogen–air mixtures

Lin Zhou (周林) ; Shengjia Tu (涂胜甲) ; Yining Zhang (张义宁)  ; Pengfei Yang (杨鹏飞)  ; Honghui Teng (滕宏辉) 

 Check for updates

Physics of Fluids 35, 116114 (2023)

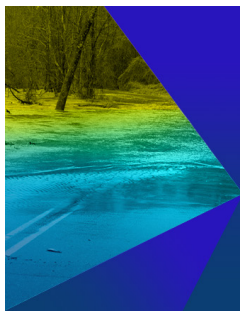
<https://doi.org/10.1063/5.0173603>



View
Online



Export
Citation



Physics of Fluids
Special Topic:
Flow and Civil Structures

Submit Today

Numerical investigation of oblique detonation waves on a truncated cone in hydrogen–air mixtures

Cite as: Phys. Fluids **35**, 116114 (2023); doi: [10.1063/5.0173603](https://doi.org/10.1063/5.0173603)

Submitted: 23 August 2023 · Accepted: 27 October 2023 ·

Published Online: 17 November 2023








View Online



Export Citation



CrossMark

Lin Zhou (周林),^{1,2}  Shengjia Tu (涂胜甲),²  Yining Zhang (张义宁),^{2,a)}  Pengfei Yang (杨鹏飞),^{3,a)} 
and Honghui Teng (滕宏辉)^{1,4} 

AFFILIATIONS

¹School of Aerospace Engineering, Beijing Institute of Technology, Beijing 100081, China

²Beijing Power Machinery Institute, Beijing 100074, China

³State Key Laboratory of High Temperature Gas Dynamics, Institute of Mechanics, Chinese Academy of Sciences, Beijing 100190, China

⁴Chongqing Innovation Center, Beijing Institute of Technology, Chongqing 401120, China

^{a)}Authors to whom correspondence should be addressed: 13718931527@163.com and young1505@foxmail.com

ABSTRACT

Traditional methods of initiating oblique detonation waves (ODWs) using wedges and cones face a fundamental challenge in reconciling the need for rapid initiation with stable combustion, especially at low flight Mach numbers ($Ma < 8$). This study introduces an innovative initiation configuration involving a truncated cone. By utilizing Euler equations coupled with detailed hydrogen–air chemical reaction models, the wave dynamics induced by the truncated cone configuration are systematically explored. The findings reveal that the truncated cone configuration enables more rapid initiation of ODWs compared to conventional cones, while also preserving improved stability when contrasted with wedge. This behavior can be attributed to the planar flow characteristics in the post-shock field of truncated cone, generated by the upstream wedge-shaped shock, and the Taylor–Maccoll flow characteristics, caused by the downstream conical shock. Furthermore, the study delves into the initiation and morphological changes with respect to the inner radius and angle of the truncated cone. As inner radii or truncated cone angle increase, three initiation wave systems emerge: stable, oscillatory, and detached modes. Analysis of the dynamic variations in pressure and velocity within the induction zone highlights that the upstream oscillation originates from the flow velocity in the induction zone falling below the local Chapman–Jouguet velocity of normal detonation wave (NDW). However, the upstream region of the truncated cone exhibits more pronounced expansion effects, leading to momentum loss, and subsequently, the weakening and even vanishing of the NDW. This prompts the downstream oscillation of the initiation structure, instigating a cyclic oscillation pattern.

Published under an exclusive license by AIP Publishing. <https://doi.org/10.1063/5.0173603>

I. INTRODUCTION

The detonation wave mainly involves two physical processes: shock waves and intense chemical reactions. It exhibits transient characteristics in time and multidimensional features in space.¹ As a pressure-gained combustion mode, detonation waves release chemical energy mainly through self-ignition induced by strong shock wave compression, exhibiting supersonic propagation and representing an efficient and rapid energy release process. Introducing detonation waves into the air-breathing scramjet engine and utilizing oblique detonation wave (ODW) to enhance the combustion efficiency can lead to the development of a new propulsion system, known as the oblique detonation engine (ODE). The mainstream of the ODE is supersonic

and the combustor size can be controlled at the centimeter level, significantly improving flight Mach number and reducing structural weight, making it a promising high-Mach number, high-specific impulse propulsion system.^{2–4}

Efficient and reliable initiation of ODW in high-speed combustible gas flows is a highly challenging task. Researchers have chosen various initiation devices to obtain oblique detonations,^{5–9} such as three typical oblique detonation initiators, i.e., blunt body, wedge, and cone. In principle, the blunt body induces strongest shock waves and is more rapidly to initiate ODWs. However, bow shock waves also cause significant total pressure losses, and downstream expansion waves strongly interact with the heat release process on the ODW front, making them

more suitable for fundamental research on detonation initiation. Lehr's study¹⁰ showed that when a projectile was injected into combustible gas at a speed close to the mixture's Chapman–Jouguet (CJ) detonation velocity, non-uniform flows induced by the blunt body shock wave led to combustion instability; increasing the flight speed can initiate detonation waves, then which gradually decayed into CJ ODWs under the action of downstream expansion waves. However, the factors determining whether the blunt body can achieve detonation initiation are not only the flight speed but also the projectile's diameter. Kasahara *et al.*¹¹ introduced a dimensionless quantity, d/λ , where d is the diameter of the spherical projectile and λ is the cell size of the incoming mixture. Detonation waves are only generated when d/λ exceeds a critical value, and this critical value decreases with an increase in the ratio of the incoming flow speed to the CJ detonation velocity. When the projectile's flight speed is approximately 1.6 times the CJ detonation velocity and d/λ is small, although the blunt body's leading edge can induce a stronger detonation wave, the shock wave front and the combustion front gradually decouple under the influence of downstream expansion waves. When d/λ is relatively large, the projectile successfully initiates ODWs, and the shock wave front downstream is tightly coupled with the combustion front. The front of the upstream detonation wave is smooth, but the downstream overdriven degree is reduced, showing small-scale wave structures.

The ODW flow field induced by a wedge mainly includes oblique shock waves (OSWs), an initiation region, and the ODW front, and this configuration is the mainstream of current ODW research. In high-speed combustible gas, the wedge first induces an OSW, and the high-temperature and high-pressure gas behind the shock wave undergoes self-ignition, eventually transforming into an ODW. According to the connection between the OSW and the ODW front, researchers classify ODWs into smooth^{12,13} and abrupt^{14,15} transition types. Figueira Da Silva and Deshaies¹⁶ attempted to distinguish these two initiation types based on the heat release time and the induction reaction time of the mixture after the oblique shock and found that when the induction time was much larger than the heat release time, the transition from OSW to ODW was abrupt. Teng and Jiang¹⁷ proposed a criterion based on the angle difference between the OSW and the ODW and suggested that a transition to the abrupt type occurred when the angle difference exceeded 15° – 18° . Furthermore, Yang *et al.*¹⁸ discovered that a subsonic region appeared downstream of the abrupt ODW, and with the decrease in flight Mach number, the area of subsonic region near the initiation region increased gradually, even leading to unsteady phenomena in the initiation region. Subsequent numerical and theoretical analyses^{19,20} indicated that the instability of the ODW initiation zone resulted mainly from the excessive compression ability of the wedge, causing the flow velocity behind the OSW to be less than the CJ detonation velocity. Thus, to expand the theoretical flight limit of the ODW, a weaker initiation method with less compression ability needs to be chosen.

The cone induces a special flow pattern, and its conical shock wave is influenced by Taylor–Maccoll flow, with the streamlines behind it gradually bending toward the cone surface, resulting in a continuous compression process. Yang *et al.*²¹ investigated two-dimensional axisymmetric ODWs induced by a cone and found that, under the same half cone/wedge angle conditions, the initiation region induced by the cone was longer, the wave front angle was lower, and the ODW front exhibited a strong coupling and decoupling flow

pattern. Han *et al.*²² numerically calculated fully three-dimensional ODWs induced by both cones and wedges. They observed that the wave front angle of the cone-induced ODW was significantly smaller than that of the wedge-induced ODW, and the cell size was larger, with a significant difference in cell shape. The reason for this phenomenon was mainly because, under the same half cone/wedge angle conditions, the compression strength of the conical shock wave was weaker than that of the wedge shock wave, resulting in a smaller overdrive degree of the conical detonation wave and a relatively larger cell size. Simultaneously, the wave front could develop more fully, generating more unsteady small-scale wave structures. However, the wave behind the conical shock wave had a lower temperature, resulting in a longer initiation distance for the ODW, making it challenging to apply directly to ODEs.

In summary, ODWs induced by bow shock waves often exhibit significant total pressure losses, and wedge-induced OSWs have a strong compression ability, but the flow velocity in the initiation region is too low to allow the stable combustion of ODWs at low Mach numbers. The compression ability of conical shock waves is too weak, leading to excessively low temperature for the downstream flow, and the initiation distance for ODWs is too long. These factors collectively hinder the engineering application of ODWs.

In this study, a novel configuration using the truncated cone is proposed to achieve both the ODW's rapid initiation and stable combustion at low-speed flight conditions. Effects of inner radius and angle of the truncated cone on ODW initiation features are investigated in detail according to realistic flight conditions. Further analysis reveals the morphological variations of the truncated cone-induced ODWs with respect to different geometric parameters and discusses the special oscillating initiation structures.

II. PHYSICAL AND NUMERICAL MODELS

Figure 1 illustrates a schematic representation of the ODW induced by a truncated cone in a combustible gas mixture. In this conceptual model, P , T , and V are the static pressure, static temperature, and velocity of the incoming flow at the combustor entrance,

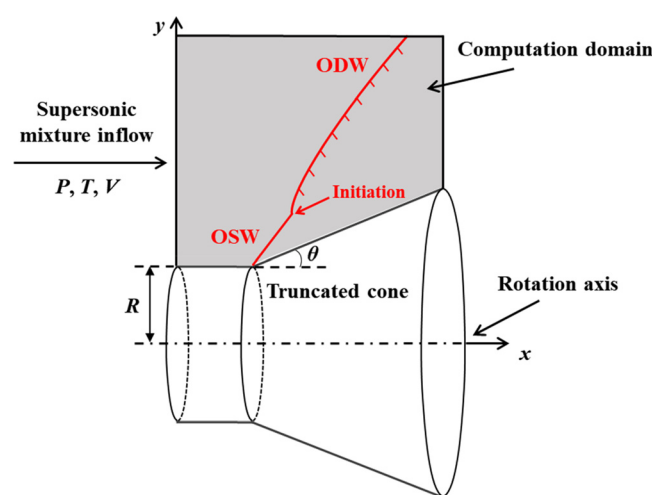


FIG. 1. Physical model and computational domain of the truncated cone-induced ODW.

respectively. The homogeneous supersonic mixture in this state interacts with the three-dimensional axisymmetric surface of the cone, resulting in the generation of axisymmetric OSW. The elevated temperature behind the OSW initiates rapid exothermic chemical reactions, culminating in the formation of an ODW downstream. The shaded area in Fig. 1 defines the computational domain employed in this investigation, as the physical configuration exhibits rotational symmetry about the x axis. Consequently, the computational model is formulated based on an axisymmetric approach. Additionally, the numerical model assumes an inviscid flow, given the relatively high Reynolds number typically encountered in scenarios involving shock-waves and detonations. Two-dimensional, axisymmetric multi-species reactive Euler equations are, therefore, used as the governing equations, i.e.,

$$\frac{\partial \mathbf{U}}{\partial t} + \frac{\partial \mathbf{F}}{\partial x} + \frac{\partial \mathbf{G}}{\partial r} + \mathbf{W} = \mathbf{S}, \quad (1)$$

where

$$\mathbf{U} = \begin{bmatrix} \rho_1 \\ \vdots \\ \rho_n \\ \rho u \\ \rho v \\ e \end{bmatrix}, \quad \mathbf{F} = \begin{bmatrix} \rho_1 u \\ \vdots \\ \rho_n u \\ \rho u^2 + p \\ \rho uv \\ (e + p)u \end{bmatrix}, \quad \mathbf{G} = \begin{bmatrix} \rho_1 v \\ \vdots \\ \rho_n v \\ \rho uv \\ \rho v^2 + p \\ (e + p)v \end{bmatrix}, \quad (2)$$

$$\mathbf{W} = \frac{v}{r} \begin{bmatrix} \rho_1 \\ \vdots \\ \rho_n \\ \rho u \\ \rho v \\ e + p \end{bmatrix}, \quad \mathbf{S} = \begin{bmatrix} \omega_1 \\ \vdots \\ \omega_n \\ 0 \\ 0 \\ 0 \end{bmatrix}.$$

Here, ρ , u , v , and p represent the density, velocity along the x axis direction, velocity along the y axis direction and pressure, respectively. r is the radius. The density ρ and the total energy e are calculated by

$$\rho = \sum_{i=1}^n \rho_i, \quad (3)$$

$$e = \rho h - p + \frac{1}{2} \rho (u^2 + v^2), \quad (4)$$

where h is the specific enthalpy, equal to $\sum_{i=1}^n \rho_i h_i / \rho$. Here, the h_i values are those calculated from the thermodynamic data for each species. The equation of state for this process is

$$p = \sum_{i=1}^n \rho_i \frac{R_0}{W_i} T, \quad (5)$$

where W_i is the molecular weight of the i th species, T is the gas temperature, R_0 is the universal gas constant, and ω_i is the mass-based rate at which the i th species is produced, which in turn is determined by the chemical reaction model. The governing equations are numerically solved by the finite-volume method. The numerical flux through each cell face is evaluated using a second-order total variation diminishing

(TVD) scheme based on an approximate Riemann solver named Harten–Lax–van Leer contact (HLLC).^{23,24} A min-mod limiter is used to suppress spurious oscillations near the discontinuities while the high-order accuracy is retained away from the jumps. The integration in time-direction is implicitly implemented via a dual time-stepping method to overcome the stiffness problem associated with solving the detailed chemical reaction processes. The Jachimowski mechanism,²⁵ which involves 19 reversible elementary reactions among nine species (H_2 , H , O_2 , O , OH , HO_2 , H_2O_2 , H_2O , and N_2) is employed to model hydrogen–air mixture combustion. The thermodynamic properties of the chemical species are evaluated using the nine-coefficient NASA polynomial representation.²⁶ The Jachimowski mechanism has been successfully applied in the previous scramjet, shock-induced combustion, and oblique detonation simulations.^{27–30}

In order to simulate the detonation combustion characteristics in real engines, inflow parameters of the ODW inside the engine combustor under realistic flight conditions are first estimated. Following the recently previous studies,^{31,32} it is assumed that the high-altitude high-speed incoming air is compressed by two equal-strength oblique shocks in the engine inlet, and the compressed static pressure, static temperature, and velocity are taken as the parameters of combustor inflow mixture for simulation calculation. Because the ODE is generally believed more suitable for high-speed flight (above Mach number 10),^{33,34} it also faces the contradiction between rapid initiation and stable combustion organization at relatively low flight Mach numbers ($Ma < 8$). Therefore, the flight Mach number of 7 and altitude of 30 km is chosen in this study to investigate the initiation and steadiness characteristics of the truncated cone-induced ODW. Using the standard atmospheric data and Rankine–Hugoniot shock relations, the process of high-altitude incoming air at flight Mach number of 7 and altitude of 30 km compressed to Mach number 3.5 through two equal-strength OSWs can be calculated. Then, the obtained static temperature, static pressure, and velocity parameters are directly used as the inflow parameters ahead the ODW combustion to carry out simulation calculation, as shown in Table I, where the equivalent ratio of mixture is taken as 0.5 with $\text{H}_2:\text{O}_2:\text{N}_2 = 1:1:3.76$.

For the simulations, the left boundary of the computational domain employs supersonic inflow conditions, fixed based on the inflow mixture parameters. These parameters are determined by the flight conditions and inlet compression. The right and upper boundaries are set as pressure outlet boundary conditions, representing high-altitude ambient static pressure. Slip wall boundary conditions are applied to both parts of the lower boundary. Initially, the entire flow field is initialized with uniform density, velocity, and pressure, calculated based on the mixture inflow conditions. In all the presented figures, the units for temperature, pressure, and density are K, kPa, and kg/m^3 , respectively.

In this research, two critical geometric parameters of the truncated cone, namely the inner radius (R) and truncated cone angle (θ),

TABLE I. Pressure, temperature, and velocity of hydrogen–air mixture at the combustor entrance with a flight Mach number of 7 and altitude of 30 km.

Mach number	Pressure (kPa)	Temperature (K)	Velocity (m/s)	CJ velocity (m/s)
3.5	29.6	709.1	1868.2	1611.1

are considered as the simulation variables, while the remaining mixture parameters (as presented in Table I) are kept constant across all simulation cases. The inner radius (R) is adjusted within the range of 0–120 mm, where the truncated cone transforms into a cone at $R=0$ mm. Furthermore, the truncated cone angle (θ) is varied between 28° and 36° to investigate its influence on the initiation characteristics of the ODWs and the morphological changes of the truncated cone.

III. RESULTS AND DISCUSSION

A. Basic structure of the truncated cone-induced ODW at low flight Mach number

This section introduces the basic flow structures of ODWs induced by a truncated cone and compares them with those induced by wedges and cones. Figure 2 shows the temperature, pressure, and OH density fields of the ODWs induced by the truncated cone, with $R=40$ mm and $\theta=30^\circ$. Similar to the ODWs induced by wedges, the truncated cone first induces an OSW, and the high-temperature gas behind it undergoes self-ignition at a certain distance, forming the ODW. The initiation region of the ODW exhibits a stable shock structure, but it lacks the distinct convergence process caused by gradual heat release, which is observed in the initiation region of the wedge-induced ODWs. Instead, a secondary normal detonation wave (NDW), nearly perpendicular to the cone surface, exists at the end of the initiation region, and it has the highest peak pressure in the entire field. Subsequently, the angle and pressure of the ODW decrease gradually, indicating a trend of decoupling between the shock and heat release surfaces, followed by re-initiation and the formation of new detonation waves. This process periodically occurs on the downstream detonation wave surface, triggering a series of triple points (TPs), and the reflected transverse waves (TWs) from these triple points directly impinge on the lower wall. This decoupling/re-coupling characteristic of the wave surfaces is similar to the flow field of ODW induced by a traditional cone,²¹ implying that the downstream flow field exhibits the cone flow characteristics.

Figure 3 shows the temperature fields of the ODWs induced by wedge and cone with the same inflow conditions and wedge/half-cone angles as in Fig. 2. For the wedge-induced ODW [Fig. 3(a)], the detonation wave first appears at $x=0.025$ m. The initiation region rapidly moves upstream, and the ODW front quickly rises, requiring only 1 ms to propagate to the entrance of the computational domain, making it impossible to be stationary on the wedge surface. Although the cone-induced ODWs can be stationary, the initiation position is too close to the downstream ($x=0.08$ m), much larger than the initiation length of the truncated cone-induced ODWs, making the initiation process very difficult and leading to a large amount of fuel being in a non-ODW combustion state.

In order to investigate the underlying physical mechanisms responsible for the relatively simpler initiation of truncated cone-induced ODWs in comparison with cone-induced ones, as well as their enhanced stability compared to wedge-induced ODWs, Figs. 4(a) and 4(b) illustrate the temperature distributions downstream of the OSWs originating from the truncated cone and cone configurations, respectively. It can be observed that the streamlines behind the OSWs of the truncated cone and cone gradually deflect toward the wall, but the deflection is more significant behind the cone-induced OSW, indicating that the flow behind the truncated cone-induced OSW also exhibits the Taylor-Maccoll effect. However, compared with the cone, the truncated cone-induced OSW has a larger angle and higher temperature. Figures 4(c) and 4(d) show the distribution characteristics of the streamline parameters. For the truncated cone-induced OSW, the temperature and pressure at the vertex are consistent with those of the wedge-induced OSW (black solid line in the figure), and then they decrease slowly but remain higher than those behind the cone-induced OSW. It is well known that the increase in temperature and pressure behind the OSW can effectively shorten the induction reaction time of the mixture and significantly reduce the initiation length of the ODW. Therefore, the truncated cone-induced OSW is easier to initiate compared to the cone-induced one.

Although the temperature and pressure at the vertex of the truncated cone-induced OSW are consistent with those of the

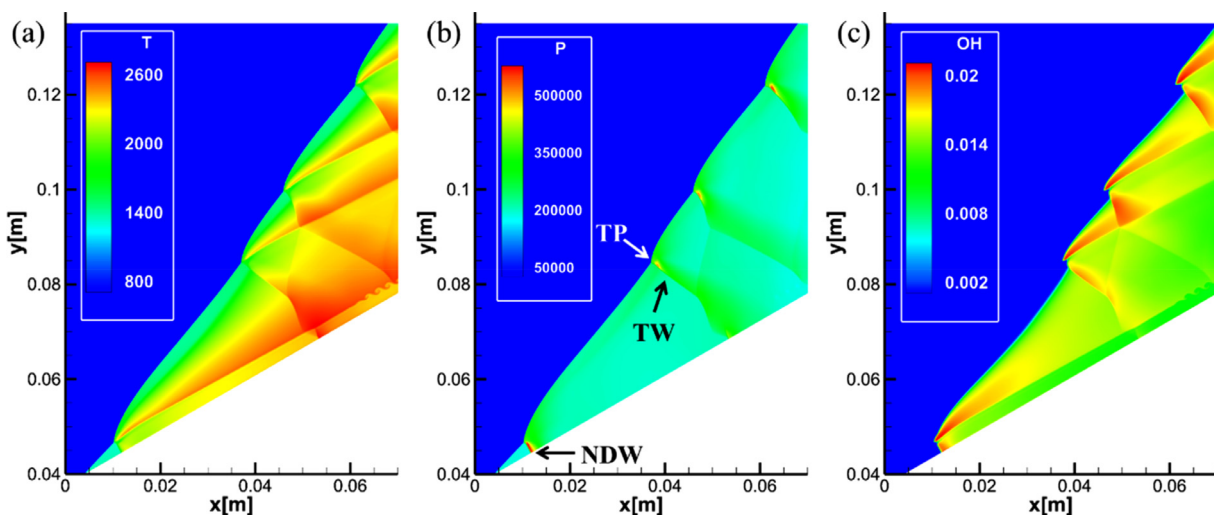


FIG. 2. Temperature (a), pressure (b), and OH density (c) fields of ODW induced by the truncated cone, $\theta=30^\circ$, $R=40$ mm.

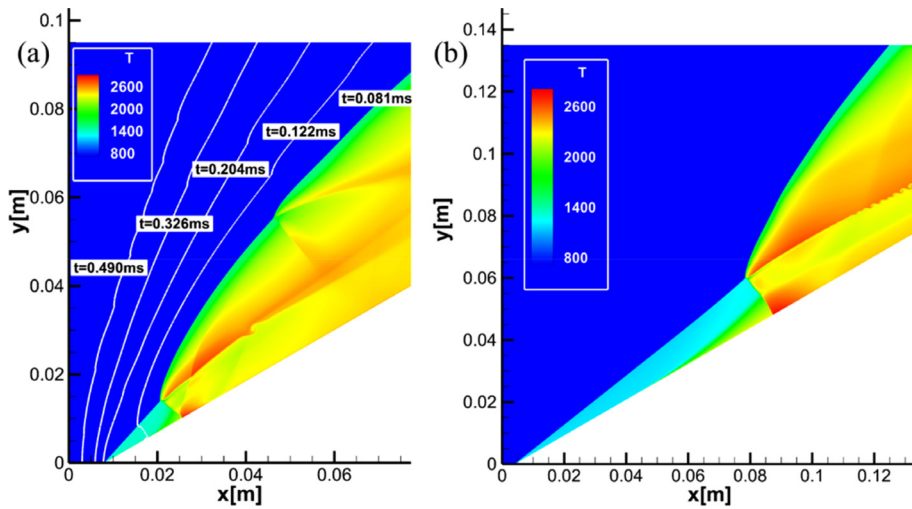


FIG. 3. Temperature fields of ODW induced by wedge (a) and cone (b); the wedge/half-cone angle θ is 30° .

wedge-induced one, the downstream flow characteristics of the truncated cone gradually approach the cone flow, and the pressure and temperature gradually decrease due to the expansion effect. Yao *et al.*^[35,36] examined the interactions of expansion waves and ODW front and found that when the downstream expansion waves directly act on the shock surface, they reduce the angle and pressure of the

shock surface, leading to the re-stationarity of the unstable ODW. Therefore, the truncated cone-induced OSW exhibits the characteristics of both wedge and cone flows. The shock strength at the vertex is the same as that of the wedge-induced OSW, effectively shortening the initiation length (compared to the cone flow). The downstream flow approaches the cone, in which the gas temperature and pressure will

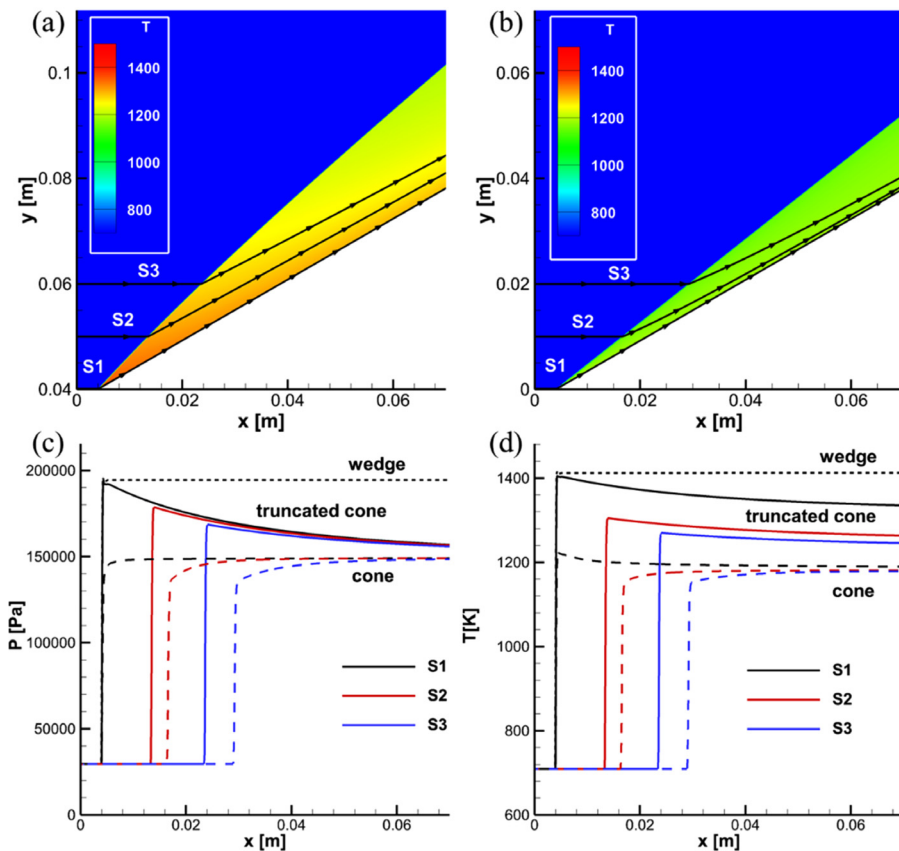


FIG. 4. Temperature fields of OSW induced by the truncated cone (a) and cone (b); pressure (c) and temperature (d) profiles along different streamlines. The wedge/half-cone angle θ is 30° , and the inner radius R is 40 mm.

08 April 2024 04:04:24

decrease gradually. Through the expansion effect, the ODWs can maintain a steady state.

B. Effects of the truncated cone inner radius

Truncated cone includes two key geometric parameters: the inner radius (R) and the truncated cone angle (θ). To investigate the effect of the truncated cone's inner radius (R) on ODWs, we varied the value of R based on the results shown in Fig. 2. Figure 5 presents the temperature, pressure, and OH density fields of the ODWs induced by the truncated cone with $R = 20$ mm. Compared to the results with $R = 40$ mm (Fig. 2), the initiation length in the $R = 20$ mm case significantly increased, with an initiation distance of approximately 0.04 m. After the OSW, a thick layer of self-ignition area exists near the wall, and a reflected shock/detonation wave forms at the connection point between the oblique shock and the ODW, interfering with the self-ignition area, creating a localized high-temperature zone near the wall. When the inner radius of the truncated cone is small, the initiation wave system of the ODW is quite similar to that induced by a cone, and the flow mechanism will be explained in Sec. III D.

As the inner radius (R) of the truncated cone increases gradually, the initiation distance of the ODWs significantly decreases, and even unsteady oscillations may occur. Figure 6 shows the temperature fields of the oscillating ODWs at different instants within one oscillation period, with an inner radius (R) of 60 mm. The black curves represent the pressure contour lines. The arrows indicate the propagation direction of the triple points, and different colors represent different triple points. At $t = 0.469$ ms, two triple points (TP1 and TP2) are present with different propagation directions: TP1 propagates upstream, and TP2 propagates downstream. At $t = 0.524$ ms, TP1 moves near the vertex of the truncated cone, then changes its direction and starts to propagate downstream, while TP2 shifts from downstream propagation to upstream propagation, and a new triple point (TP3) appears downstream of the ODW. Subsequently, TP3 starts propagating upstream, and TP1 undergoes a secondary change in direction, propagating

upstream again, as shown in Fig. 6(c). At $t = 0.649$ ms, TP1 undergoes a third change in direction and gradually disappears as it is swallowed by TP2. TP2 continues propagating upstream, and TP3 changes its direction, continuing the process described above. In one complete oscillation cycle, TP1 undergoes three changes in propagation direction and eventually disappears, while TP2 undergoes two changes in propagation direction and eventually replaces the original TP1's position, starting the next cycle.

By further increasing the inner radius of the truncated cone to 120 mm, the ODW enters a detached state and exhibits non-stationary oscillations. The oscillations in this type of wave system mainly arise from the continuous upstream propagation of the wavefront's triple point, leading to interactions with the truncated cone's apex, as illustrated in the pressure field of the ODW shown in Fig. 7. When the local wavefront angle of the ODW becomes relatively large, the transverse flow velocity behind the wavefront decreases, even becoming smaller than the transverse wave's propagation velocity. Under such circumstances, the triple point moves upstream, and for a more detailed explanation, reference can be made to previous literature.³⁷

C. Effects of the truncated cone angle

When the truncated cone angle (θ) of the truncated cone is decreased from 30° to 28° (Fig. 8), the initiation length of the ODW is significantly increased. This is mainly attributed to the decrease in temperature behind the OSW, resulting in a longer induction reaction time of the shocked mixture. Although the downstream detonation wave front is more curved, no triple points present in the current computational domain. The ODW is successfully initiated at approximately $x = 0.025$ m, and after initiation, the ODW front angle and pressure display a phenomenon of first decreasing and then increasing. This phenomenon is also observed in the OH density field shown in Fig. 8(c), indicating that the distance between the shock front and the reaction front increases after initiation, displaying a mild decoupling, and the strength of the detonation wave weakens.

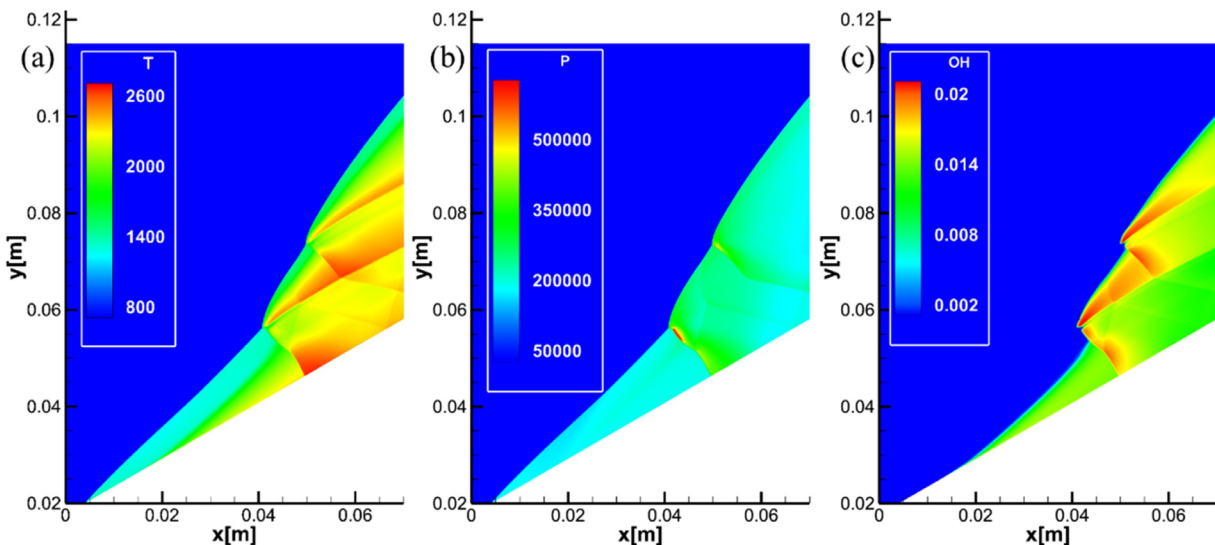


FIG. 5. Temperature (a), pressure (b), and OH density (c) fields of ODW induced by the truncated cone, $\theta = 30^\circ$, $R = 20$ mm.

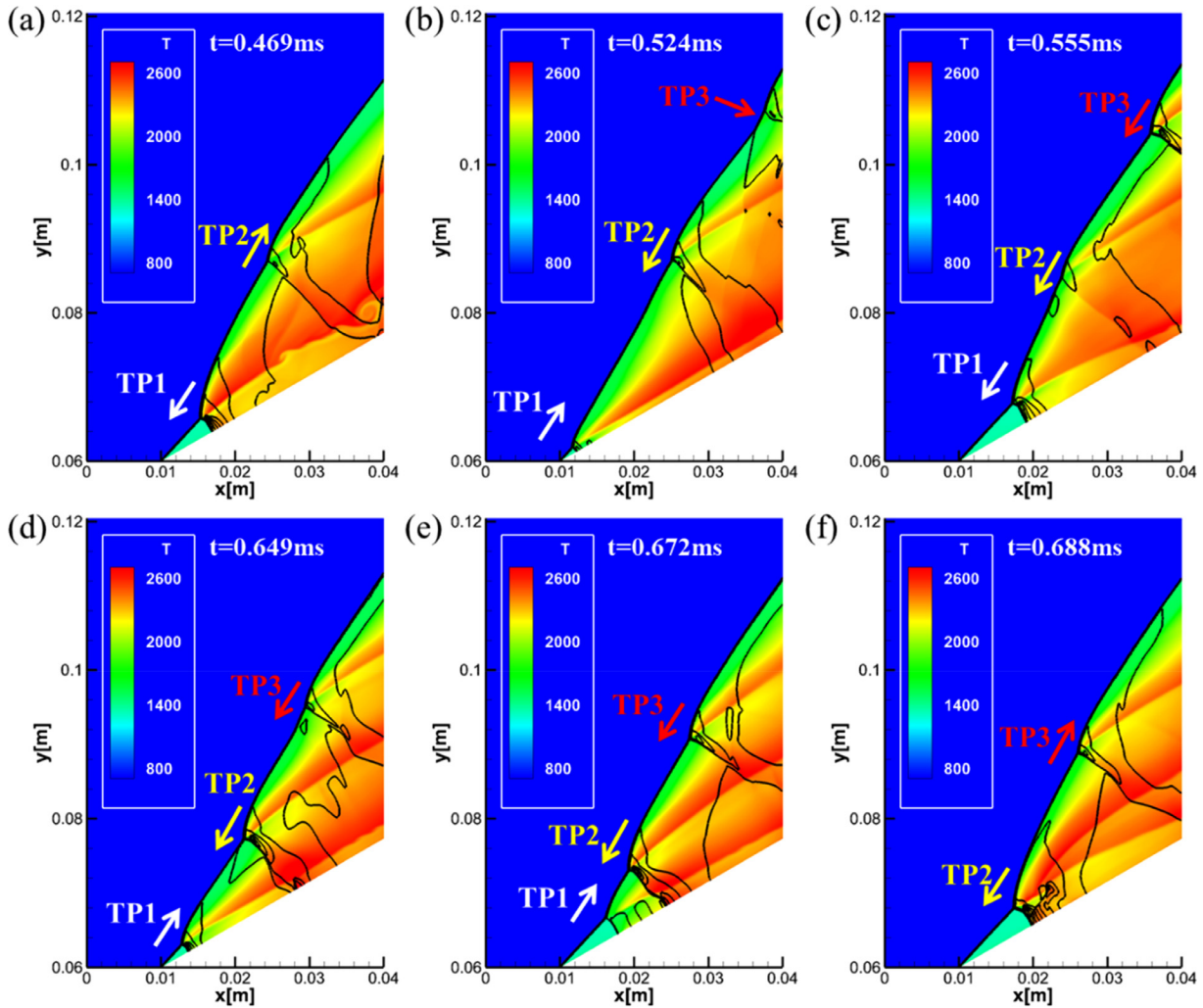


FIG. 6. Temperature fields of the oscillating ODWs at different instants, $\theta = 30^\circ$, $R = 60$ mm, $t =$ (a) 0.469, (b) 0.524, (c) 0.555, (d) 0.649, (e) 0.672, and (f) 0.688 ms.

Figure 9 shows the temperature fields of the ODWs at different instants, with a truncated cone angle of 32° . Similar to the results with a large inner radius, non-steady oscillations occur in the ODWs when the truncated cone angle is relatively large. From Figs. 9(a)–9(c), it can be observed that the triple point (TP) and the NDW at the end of the initiation region move upstream. When reaching the vertex of the truncated cone, the propagation direction of the ODW changes, and the detonation wave starts propagating downstream [see Fig. 9(b)]. It should be noted that the transition from the OSW to the ODW is achieved through a curved smooth shock, not initially through the triple points. During the downstream propagation of the ODW, new detonation waves and triple points form at the end of the initiation region, triggering the next cycle of upstream propagation [Fig. 9(f)]. This non-steady oscillation behavior is similar to that shown in Fig. 6, mainly due to the continuous propagation and strength variation of the NDW in the initiation region behind the OSW.

Continuously increasing the truncated cone angle, detachment behavior of the ODW is also observed, and the relevant results are

shown in Fig. 10. The figure displays the ODW surfaces at two different instants, illustrating the oscillation amplitude of the ODW. However, the existence of triple points propagating upstream mainly causes the unsteady oscillation of the wave system, which is attributed to their collision with the vertex of the truncated cone. This behavior is similar to that shown in Fig. 7, where the results were obtained by increasing the inner radius of the truncated cone.

In summary, the effects of increasing the truncated cone angle and inner radius on ODWs are essentially consistent, mainly manifested in the following aspects: first, a significant decrease in initiation distance; second, the occurrence of unsteady wave system oscillations under specific truncated cone angles and inner radii; third, detachment behavior of the ODW induced by excessively large truncated cone angles or inner radii. According to the wave systems presented above, the three typical morphologies of ODWs induced by the truncated cone are illustrated in Fig. 11. Among them, the black line represents the leading shock wave, and the red line represents the chemical reaction front. The blue line in Figs. 11(b) and 11(c) represents the leading

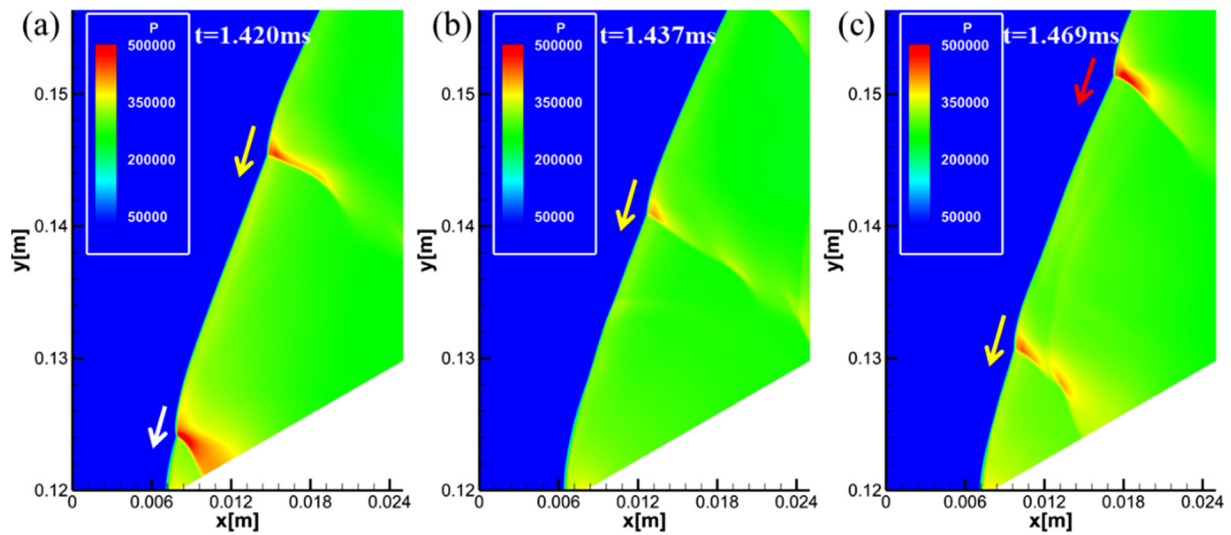


FIG. 7. Pressure fields of ODW induced by the truncated cone, $\theta = 30^\circ$, $R = 120$ mm, $t =$ (a) 1.420, (b) 1.437, and (c) 1.469 ms.

shock wave of the oscillating initiation structure at another instant, which differs from the black lines during the oscillation period. When the truncated cone angle and inner radius of the truncated cone are relatively small, a self-ignition region exists behind the OSW, and a reflected shock/detonation wave interferes with the self-ignition region at the connection point between the OSW and the ODW. It is noteworthy that, in this scenario, the main triple point remains stable (connecting the OSW and ODW), while the others TPs moves downstream. As the truncated cone angle or inner radius of the truncated cone increases, the strength of the OSW is enhanced, leading to a shorter initiation distance. The NDW in the initiation zone undergoes forward and backward movements, causing transitions between smooth and abrupt changes in the initiation wave system. The oscillations appear in the positions of the triple points along the wave front.

Continuously increasing the truncated cone angle or inner radius of the truncated cone results in a large subsonic region behind the wave, triggering the detachment behavior of the ODW, and the triple points continue to propagate upstream along the wavefront, leading to unsteady oscillations of the wave. It should be noted that the detached ODWs (type III) will maintain sustained oscillation rather than continuously propagating upstream. However, if the inner radius R of the truncated cone increases to infinity, it can be deduced that the induced ODWs cannot maintain stationary, which is similar to the case shown in Fig. 3(a). The reason is that the truncated cone tends to approach the configuration of wedge, which leads negligible expansion effect downstream the truncated cone. Therefore, the detached ODWs will propagate to the entrance of the computational domain at this time, which cannot maintain stationary on the truncated cone surface.

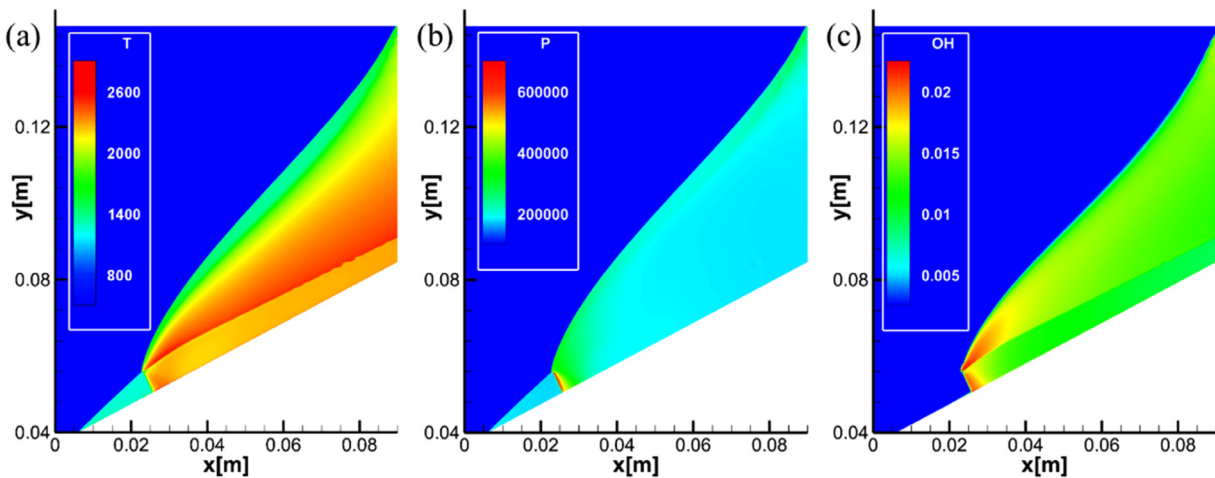


FIG. 8. Temperature (a), pressure (b), and OH density (c) fields of ODW induced by the truncated cone, $\theta = 28^\circ$, $R = 40$ mm.

08 April 2024 04:04:24

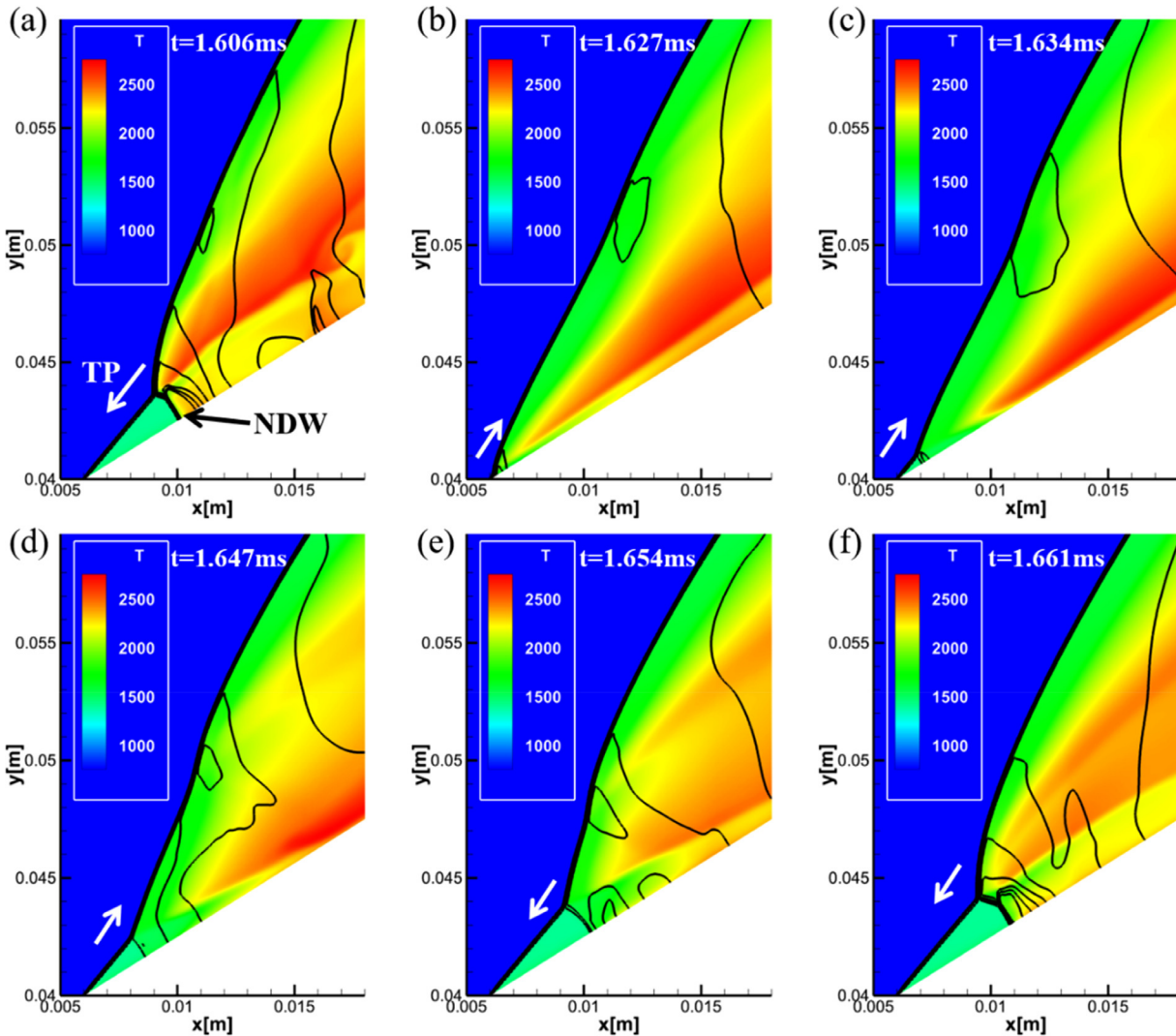


FIG. 9. Temperature fields of ODW induced by the truncated cone, $\theta = 32^\circ$, $R = 40$ mm, $t =$ (a) 1.606, (b) 1.627, (c) 1.634, (d) 1.647, (e) 1.654, and (f) 1.661 ms.

D. Analysis of initiation characteristics of the truncated cone ODWs

To quantitatively analyze the initiation characteristics of ODWs induced by the truncated cone, we conducted statistical analyses of the effects of the truncated cone angle and inner radius on the initiation distance, and the results are presented in Fig. 12, with error bars representing the oscillation range of initiation distance for unsteady cases. For attached detonation waves [as shown in Figs. 11(a) and 11(b)], the initiation distance is defined as the length from the beginning of the truncated cone to the triple point along the truncated cone direction, and this length is defined as positive. For detached detonation waves [as shown in Fig. 11(c)], the initiation distance is defined as the length by which the detonation wave detaches from the starting point of the truncated cone, and this length is defined as positive. The trends of the initiation distance variation are similar under different truncated cone

angles and inner radii of the truncated cone. With increasing truncated cone angle and inner radius, the initiation distance gradually decreases, and the initiation wave system experiences transitions between steady state, small-amplitude oscillations, large-amplitude oscillations, and then back to small-scale oscillations, ultimately leading to detached behavior of ODWs.

As the truncated cone angle of the truncated cone is increased, the strength of the induced shock is enhanced, leading to higher post-shock temperatures and a shorter initiation distance. This explanation is straightforward. However, it is an interesting question why increasing the inner radius (R) of the truncated cone also leads to similar phenomena. To explore this, we disregarded the effect of chemical reactions and plotted the pressure and Mach number distributions along the truncated cone surface for different inner radii (R), as shown in Fig. 13. In fact, a wedge can be considered as a truncated cone with

08 April 2024 04:04:24

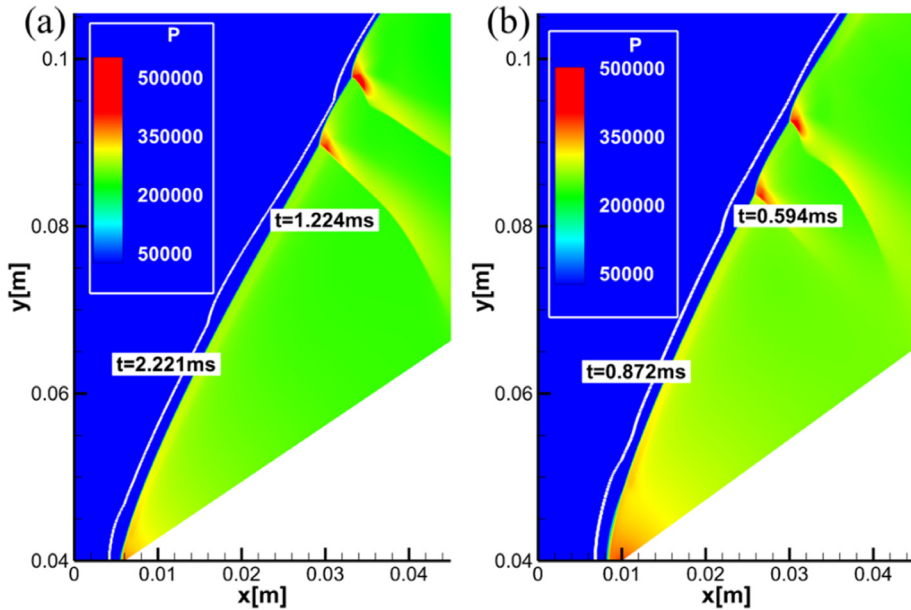


FIG. 10. The truncated cone-induced ODW, $R = 40$ mm, $\theta = 34^\circ$ (a) and $\theta = 36^\circ$ (b); white lines show the wave surfaces of the detached ODWs at the most forward positions during the oscillation period.

an infinite inner radius, and a cone can be viewed as a truncated cone with an R of 0. It can be observed that as the inner radius of the truncated cone increases, the pressure/Mach number distribution gradually shifts from the conical flow to the wedge flow. The high-temperature and high-pressure region behind the shock increases gradually, resulting in higher temperatures and pressures of the mixed gas. Therefore, the increase in the inner radius effectively shortens the initiation distance of the ODW due to the increase in the mixture temperature and pressure. Additionally, we found that the flow over the truncated cone is non-uniform. As the flow moves downstream, there is a strong expansion effect (pressure reduction), and this effect becomes more pronounced as it approaches the vertex of the truncated cone (large pressure gradient changes). This is also the reason why ODWs induced

by the truncated cone mostly reside near the vertex of the truncated cone. This behavior is similar to the detached ODW caused by the wedges, where the ODW can re-stabilize downstream under the action of the expansion effect.³⁶

The reason for the periodic oscillations of the steady inflow-induced ODWs is an interesting question for exploration. Teng *et al.*²⁰ conducted research on the stable boundary of ODWs at high altitudes and found that secondary NDWs appear in the initiation region at low Mach numbers. If the local flow velocity in the initiation zone is less than the local CJ detonation velocity of the mixture, the NDW in the initiation zone cannot be stationary and propagates upstream, resulting in the overall instability of the ODW. Therefore, we measured the Mach numbers of the post-shock mixtures compressed by the wedge

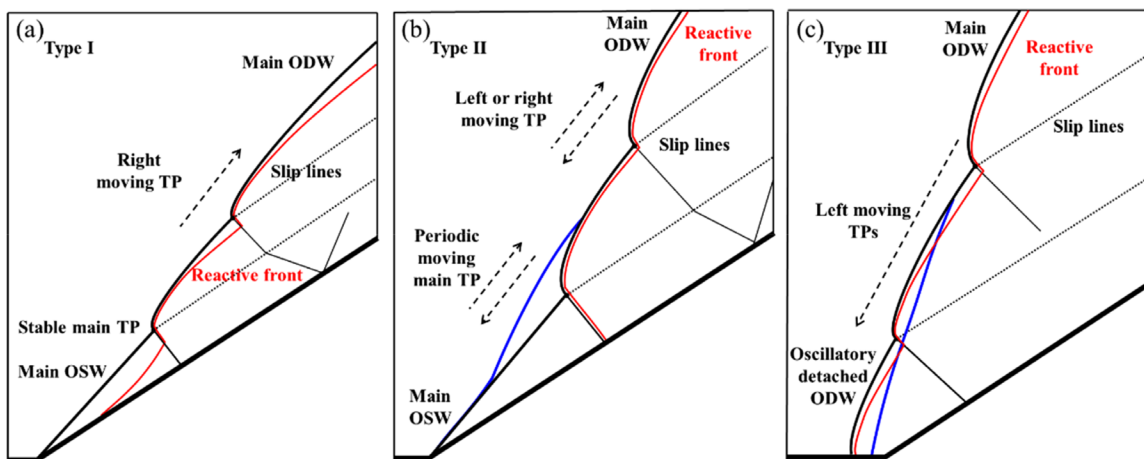


FIG. 11. Morphology of the truncated cone ODWs and blue lines show the leading shock wave structures at another instance during the oscillation period. The ODW morphology types are named as (a) type I, (b) type II, and (c) type III, respectively.

08 April 2024 04:04:24

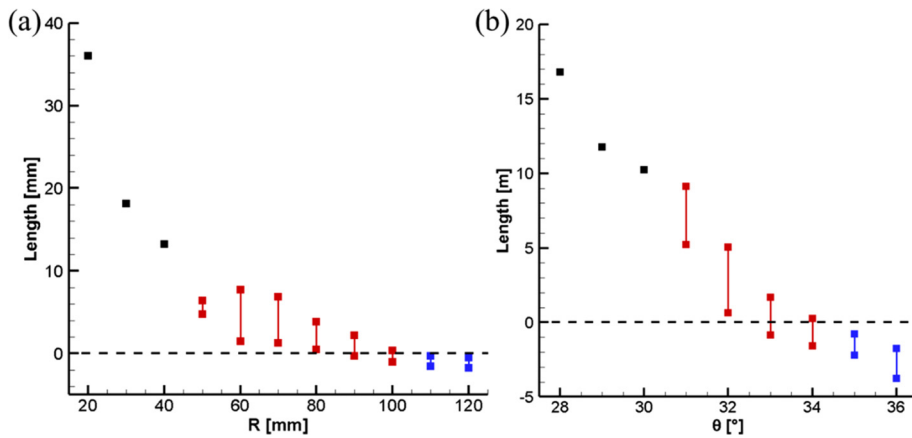


FIG. 12. Comparison of initiation distance under different truncated cone radius (a) and angles (b).

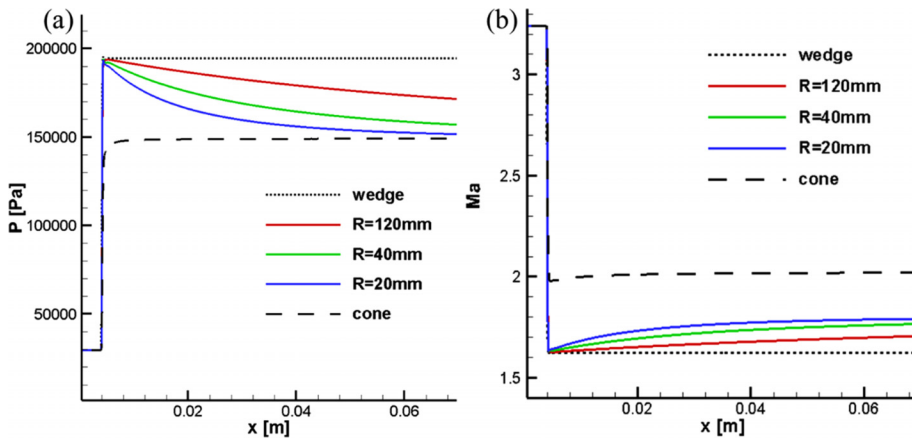


FIG. 13. Pressure (a) and Mach number (b) distributions along $y = 0$ mm streamline of wedge, truncated cone and cone-induced OSW flow field with the wedge/half cone angle $\theta = 30^\circ$.

and cone; and theoretically calculated the corresponding local CJ Mach number of the detonation wave. The results are shown in Fig. 14.

It should be noted that the post shock parameters of the cone-induced OSW are inhomogeneous due to the Taylor-Maccoll effect. The two Mach numbers of the cone are calculated according to the parameters of the cone surface. The dashed lines represent the theoretical CJ velocity, and the solid lines represent the flow velocity. It can be observed that the flow velocity is consistently lower than the theoretical CJ detonation velocity. According to previous research,^{38–40} all the cases in this study would exhibit detached ODWs propagating continuously upstream, as shown for the cases with the wedge, e.g., Fig. 3(a). However, for the cases with the truncated cone and the cone, even when the theoretical CJ velocity of the detonation wave is greater than the local flow velocity, the ODW may still be stationary. The main reason for this phenomenon is that the post-shock flow parameters of the truncated cone are non-uniform, and the expansion effect behind the oblique shock results in a loss of momentum, weakening the detonation wave behind the oblique shock and reducing the theoretical propagation speed of the NDW. This is only a qualitative explanation, and further detailed quantitative analysis is necessary in the future.

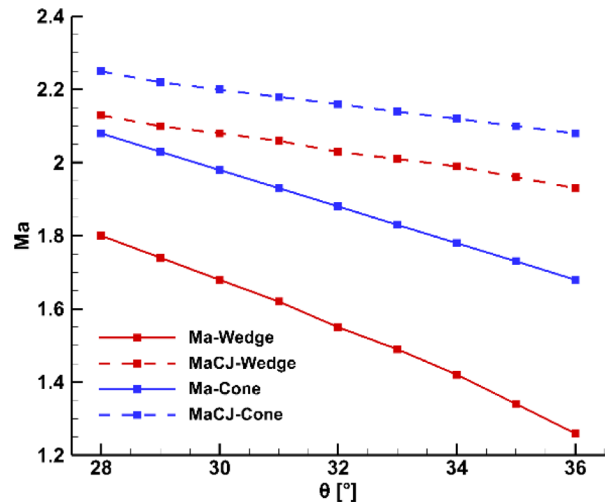


FIG. 14. Local Mach number and local CJ Mach number of the post shock mixtures compressed by the wedge and cone with different wedge angles and half cone angles.

08 April 2024 04:04:24

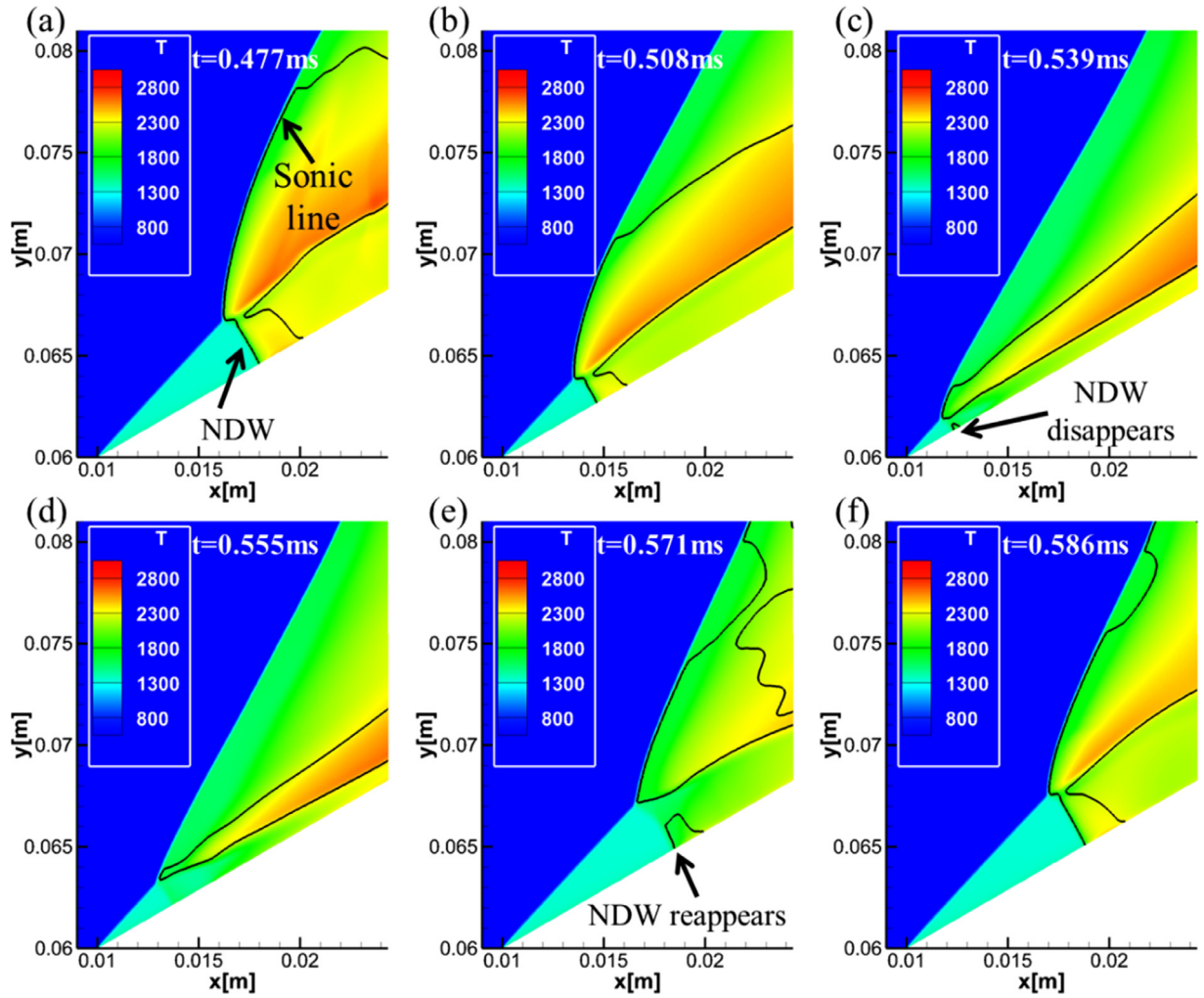


FIG. 15. Temperature with black sonic lines of periodic oscillatory initiation zone, $\theta = 30^\circ$, $R = 60$ mm, $t =$ (a) 0.477, (b) 0.508, (c) 0.539, (d) 0.555, (e) 0.571, and (f) 0.586 ms.

Nonetheless, the stable phenomenon differs from previous studies is first discovered and addressed.

To verify the above analysis, Fig. 15 presents the temperature field and subsonic region near the initiation zone at different instants, with an inner radius (R) of 60 mm and a truncated cone angle (θ) of 30° . It can be observed that when NDW appears downstream in the initiation zone, it propagates upstream, gradually decreases in height, and weakens in strength [Figs. 15(a) and 15(b)]. When it approaches the vertex of the truncated cone, the NDW almost disappears [Fig. 15(c)]. At this point, the high-speed flow behind the oblique shock will push the detonation wave downstream, and a new NDW forms and then starts propagating upstream in the downstream region, as shown in Figs. 15(d)–15(f). To further quantitatively demonstrate the process of periodic oscillation, the pressure distributions on the truncated cone surface at different instants are extracted and shown in Fig. 16. From the large fluctuations of pressure peaks, it can be seen that the strength of the NDW in the initiation zone exhibits significant variations during the periodic oscillations.

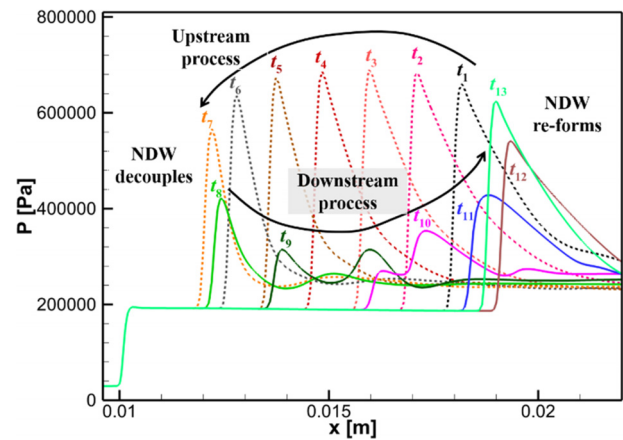


FIG. 16. Pressure profiles along the cone surface at different times, $\theta = 30^\circ$, $R = 60$ mm.

As indicated by the high-pressure peaks from Fig. 16, when the NDW is stronger, the CJ velocity even with the expansion effect, exceeds the local flow velocity, resulting in the upstream propagation of the initiation structure. According to the evidence from the pressure change curve in Fig. 13(a), the closer to the upstream region of the truncated cone, the greater the rate of pressure change, indicating a stronger expansion effect of the truncated cone. As the ODW gradually propagates upstream further, the expansion effect becomes stronger. The subsonic regions behind the ODW and NDW decrease gradually as the upstream movement. Upon reaching the uppermost position, the subsonic regions behind the ODW and NDW become fully decoupled, and the NDW also disappears [Fig. 15(c)]. It is well known that traditional combustion modes struggle to maintain stability in such high-speed airflow. Hence, the self-ignition point in the induction zone progressively moves downstream. During the downstream process, the expansion effect weakens, leading to the gradual enlargement of the subsonic region caused by the heat release, eventually merging with the subsonic region behind the ODW. Simultaneously, a new NDW forms [Fig. 15(e)], initiating the next oscillation cycle. Figure 16 quantitatively illustrates the evolution of surface pressure on the truncated cone, clearly depicting the disappearance and formation processes of the NDW in the induction zone.

IV. CONCLUSION

The numerical investigation delved into the initiation and morphological characteristics of ODWs induced on the truncated cone within a stoichiometric hydrogen–air mixture. Traditionally, ODWs have been initiated using wedges or cones, yet they grapple with the dual challenge of achieving rapid initiation and maintaining stable combustion at relatively low flight velocities within engines. This study introduced a novel approach by simulating the initiation of ODWs on a truncated cone at a flight Mach number of 7, utilizing the control parameters R and θ .

The study's findings have illuminated that truncated cone-induced ODWs exhibit a distinct advantage of rapid initiation and heightened stability when compared to conventional initiation methods, specifically cones and wedges. This unique behavior can be attributed to the dual-flow characteristics of the truncated cone-induced flow, where the upstream shock wave on the truncated cone exhibits features similar to those induced by a wedge, while the downstream shock wave resembles those induced by a conical shape. This configuration relies on the strong shock wave for rapid initiation and capitalizes on flow expansion effects for sustained detonation stability. These special characteristics bring the unique advantage of the truncated cone-induced ODW, which is more likely to be stationary than the wedge-induced ODW. Therefore, for engineering applications of ODE, the truncated cone-induced ODW can provide an effective way for low Mach number flight, which broadens the lower limit of the ODE flight speed range. In addition, compared with the traditional rectangular combustor configuration, the axially symmetric combustor configuration can relatively reduce the difficulty of thermal protection, which is more conducive to the future engineering applications. Furthermore, ODE using the truncated cone to organize ODW provides a new solution to combine with the rotating detonation engine to construct a novel air-breathing combined detonation engine with wide speed range and high performance, which presents broad application prospects.

Furthermore, the investigation has revealed that the effects of the truncated cone angle and inner radius on ODWs maintain a consistent

pattern. These effects are primarily demonstrated in three key aspects: a substantial reduction in initiation distance, the emergence of unsteady wave system oscillations under specific truncated cone angles and inner radii, and the detachment behavior of the ODW induced by excessive truncated cone angles or inner radii. Notably, the intense periodic oscillations observed in the ODW wave system under moderate inner radii and truncated cone angles are closely intertwined with the intricate flow characteristics of the truncated cone-induced flow. In essence, this research not only offers valuable insights into the flows of truncated cone-induced ODWs but also presents a promising avenue for enhanced applications of ODWs technology. The elucidation of these underlying dynamics serves to further advance our understanding of detonation instabilities, opening doors for optimized engineering solutions in the realm of detonation propulsion systems.

ACKNOWLEDGMENTS

This research was supported by the National Natural Science Foundation of China (Nos. 12202014 and 12325206).

AUTHOR DECLARATIONS

Conflict of Interest

The authors have no conflicts to disclose.

Author Contributions

Lin Zhou: Data curation (equal); Formal analysis (equal); Investigation (equal); Writing – original draft (equal); Writing – review & editing (equal). **Shengjia Tu:** Formal analysis (equal); Methodology (equal). **Yining Zhang:** Conceptualization (equal); Investigation (equal); Supervision (equal); Writing – review & editing (equal). **Pengfei Yang:** Formal analysis (equal); Writing – original draft (equal); Writing – review & editing (equal). **Honghui Teng:** Conceptualization (equal); Supervision (equal).

DATA AVAILABILITY

The data that support the findings of this study are available from the corresponding author upon reasonable request.

APPENDIX: THE EFFECT OF GRID RESOLUTION

In order to eliminate the influence of grid size on the simulation results of the truncated cone-induced ODWs, resolution studies are also conducted by refining the computational mesh in each axis direction. For instance, the temperature field in the case of $\theta = 30^\circ$ and $R = 40$ mm generated using the default average mesh size $50 \mu\text{m}$ is presented in Fig. 17, compared with the simulation result obtained by a finer average mesh size $30 \mu\text{m}$. Since the simulation cases of this paper correspond to the high-altitude flight conditions, the inflow density is relatively low, and the temperature is high, convergence of the ODW flow field simulation does not require a very dense mesh. For the aforementioned case, there are approximately 200 grids in the induction zone of the ODW. It is evident that there is negligible difference between the two wave structures with different grid length scales including the ODW angle, initiation location, and triple points inside the computational domain.

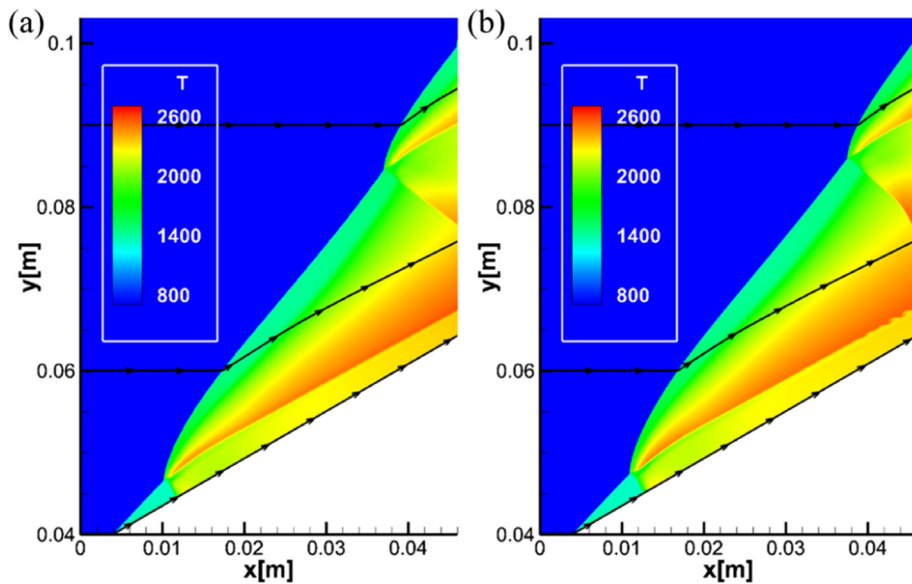


FIG. 17. Temperature fields of $\theta = 30^\circ$, $R = 40$ mm case with different mesh sizes (a) average mesh size 0.03 mm and (b) average mesh size 0.05 mm.

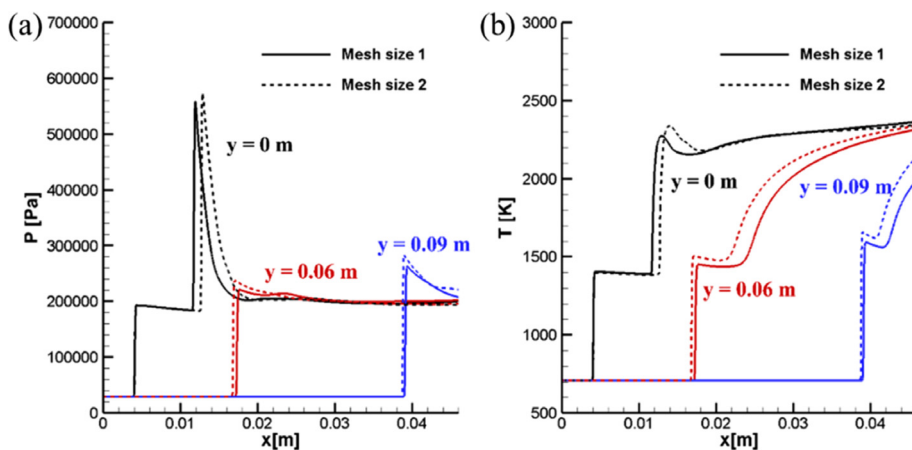


FIG. 18. (a) Pressure and (b) temperature of $\theta = 30^\circ$, $R = 40$ mm case along different streamlines with different mesh sizes (mesh size 1: average mesh size 0.03 mm, mesh size 2: average mesh size 0.05 mm).

The additional quantitative comparisons shown in Fig. 18 provide the detailed distributions of pressure and temperature along three typical lines (i.e., $y = 0.04, 0.06$, and 0.09 m) corresponding to different regions of the truncated cone-induced ODW include the OSW and ODW surface. Although a very little discrepancy appears in the parameter-specific values and locations on the shock wave surfaces which can be due to the unsteadiness of the ODW structure as well, the curves having different grid scales can be seen to almost coincide with one another. For the purpose of this work, the default mesh size used in this case is seen to be sufficient to capture the main features of the ODW structure. For other cases with different θ and R , similar resolution studies have been performed to confirm the grid-independence of the simulation results in this study.

REFERENCES

¹J. E. Shepherd, “Detonation in gases,” *Proc. Combust. Inst.* **32**, 83–98 (2009).
²J. L. Cambier, H. Adelman, and G. P. Menees, “Numerical simulations of an oblique detonation wave engine,” *J. Propul. Power* **6**, 315–323 (1990).

³D. T. Pratt, J. W. Humphrey, and D. E. Glenn, “Morphology of standing oblique detonation waves,” *J. Propul. Power* **7**(5), 837–845 (1991).
⁴P. Wolański, “Detonative propulsion,” *Proc. Combust. Inst.* **34**, 125–158 (2013).
⁵A. A. Vasiljev, “Initiation of gaseous detonation by a high speed body,” *Shock Waves* **3**, 321–326 (1994).
⁶J. Verreault and A. J. Higgins, “Initiation of detonation by conical projectiles,” *Proc. Combust. Inst.* **33**(2), 2311–2318 (2011).
⁷J. M. Powers and K. A. Gonthier, “Reaction zone structure for strong, weak overdriven, and weak underdriven oblique detonations,” *Phys. Fluids* **4**(9), 2082–2089 (1992).
⁸K. Iwata, “Numerical approach to theoretical aspects of wedge-induced oblique detonation wave in a hydrogen concentration gradient,” *Phys. Fluids* **35**(7), 076121 (2023).
⁹Z. Luan, Y. Huang, R. Deiterding, and Y. You, “On the evolutions of triple point structure in wedge-stabilized oblique detonations,” *Phys. Fluids* **34**(6), 067118 (2022).
¹⁰H. F. Lehr, “Experiment on shock-induced combustion,” *Astronaut. Acta* **14**(4–5), 589–597 (1972).
¹¹J. Kasahara, T. Arai, S. Chiba, K. Takazawa, Y. Tanahashi, and A. Matsuo, “Criticality for stabilized oblique detonation waves around spherical bodies in acetylene/oxygen/krypton mixtures,” *Proc. Combust. Inst.* **29**, 2817–2824 (2002).

08 April 2024 04:04:24

- ¹²T. Wang, Y. Zhang, H. Teng, Z. Jiang, and H. D. Ng, "Numerical study of oblique detonation wave initiation in a stoichiometric hydrogen-air mixture," *Phys. Fluids* **27**, 096101 (2015).
- ¹³G. Q. Zhang, S. F. Gao, and G. X. Xiang, "Study on initiation mode of oblique detonation induced by a finite wedge," *Phys. Fluids* **33**(1), 016102 (2021).
- ¹⁴C. Li, K. Kailasanath, and E. S. Oran, "Detonation structures behind oblique shocks," *Phys. Fluids* **6**, 1600–1611 (1994).
- ¹⁵C. Viguier, L. F. Figueira Da Silva, D. Desbordes, and B. Deshaies, "Onset of oblique detonation waves: Comparison between experimental and numerical results for hydrogen-air mixture," *Symp. (Int.) Combust.* **26**, 3023–3031 (1996).
- ¹⁶L. F. Figueira Da Silva and B. Deshaies, "Stabilization of an oblique detonation wave by a wedge: A parametric numerical study," *Combust. Flame* **121**, 152–166 (2000).
- ¹⁷H. H. Teng and Z. L. Jiang, "On the transition pattern of the oblique detonation structure," *J. Fluid Mech.* **713**, 659 (2012).
- ¹⁸P. Yang, H. Teng, Z. Jiang, and H. D. Ng, "Effects of inflow Mach number on oblique detonation initiation with a two-step induction-reaction kinetic model," *Combust. Flame* **193**, 246–256 (2018).
- ¹⁹H. Teng, C. Tian, Y. Zhang, L. Zhou, and H. D. Ng, "Morphology of oblique detonation waves in a stoichiometric hydrogen-air mixture," *J. Fluid Mech.* **913**, A1 (2021).
- ²⁰H. Teng, J. Bian, L. Zhou, and Y. Zhang, "A numerical investigation of oblique detonation waves in hydrogen-air mixtures at low Mach numbers," *Int. J. Hydrogen Energy* **46**, 10984–10994 (2021).
- ²¹P. Yang, H. D. Ng, H. Teng, and Z. Jiang, "Initiation structure of oblique detonation waves behind conical shocks," *Phys. Fluids* **29**, 086104 (2017).
- ²²W. Han, C. Wang, and C. K. Law, "Three-dimensional simulation of oblique detonation waves attached to cone," *Phys. Rev. Fluids* **4**(5), 053201 (2019).
- ²³S. Chakravarthy, "A unified-grid finite volume formulation for computational fluid dynamics," *Int. J. Numer. Methods Fluids* **31**(1), 309–323 (1999).
- ²⁴E. F. Toro, *Riemann Solvers and Numerical Methods for Fluid Dynamics: A Practical Introduction* (Springer Science & Business Media, 2013).
- ²⁵C. J. Jachimowski, "An analytical study of the hydrogen-air reaction mechanism with application to scramjet combustion," Technical Report No. NASA-TP-2791 (NASA Langley Research Center, 1988).
- ²⁶B. J. McBride, M. J. Zehe, and S. Gordon, "NASA Glenn coefficients for calculating thermodynamic properties of individual species," Technical Report No. NASA/TP-2002-211556 (NASA Glenn Research Center, 2002).
- ²⁷M. Chapuis, E. Fedina, C. Fureby, K. Hannemann, S. Karl, and J. Martinez Schramm, "A computational study of the Hyshot II combustor performance," *Proc. Combust. Inst.* **34**(2), 2101–2109 (2013).
- ²⁸J. Y. Choi, I. S. Jeung, and Y. Yoon, "Computational fluid dynamics algorithms for unsteady shock-induced combustion," *AIAA J.* **38**(7), 1179–1187 (2000).
- ²⁹J. Y. Choi, E. J. R. Shin, and I. S. Jeung, "Unsteady combustion induced by oblique shock waves at the non-attaching condition of the oblique detonation wave," *Proc. Combust. Inst.* **32**(2), 2387–2396 (2009).
- ³⁰H. Xiong, R. Qiu, X. Han, H. Yan, and Y. You, "Investigating the flow characteristics and thermodynamic performance of curved detonation waves," *Phys. Fluids* **35**(8), 087119 (2023).
- ³¹J. Bian, L. Zhou, and H. Teng, "Structural and thermal analysis on oblique detonation influenced by different forebody compressions in hydrogen-air mixtures," *Fuel* **286**, 119458 (2021).
- ³²X. Shi, H. Xie, L. Zhou, and Y. Zhang, "A theoretical criterion on the initiation type of oblique detonation waves," *Acta Astronaut.* **190**, 342–348 (2022).
- ³³S. A. Ashford and G. Emanuel, "Oblique detonation wave engine performance prediction," *J. Propul. Power* **12**, 322–327 (1996).
- ³⁴J. Chan and J. P. Sislian, "Numerically simulated comparative performance of a scramjet and shcramjet at Mach 11," *J. Propul. Power* **26**, 1125–1134 (2010).
- ³⁵K. Yao, C. Wang, and Z. Jiang, "A numerical study of oblique detonation re-stabilization by expansion waves," *Aerosp. Sci. Technol.* **122**, 107409 (2022).
- ³⁶K. Yao, P. Yang, H. Li, C. Wang, and Z. Jiang, "Characteristics of reattached oblique detonation induced by a double wedge," *Phys. Fluids* **35**(3), 036112 (2023).
- ³⁷P. Yang, H. Li, Z. Chen, C. Wang, and H. Teng, "Numerical investigation on movement of triple points on oblique detonation surfaces," *Phys. Fluids* **34**, 066113 (2022).
- ³⁸Y. Liu, W. Chen, L. Wang, B. Xiao, and X. Cai, "Oblique detonation initiation by an instantaneous energy source in high-speed wedge flows," *AIAA J.* **59**(11), 4794–4799 (2021).
- ³⁹Y. Liu, D. Wu, S. Yao, and J. P. Wang, "Analytical and numerical investigations of wedge-induced oblique detonation waves at low inflow Mach number," *Combust. Sci. Technol.* **187**, 843–856 (2015).
- ⁴⁰H. Teng, Y. Zhang, and Z. Jiang, "Numerical investigation on the induction zone structure of the oblique detonation waves," *Comput. Fluids* **95**, 127–131 (2014).